Journal of Alloys and Compounds 509 (2011) 3559–3565

Contents lists available at ScienceDirect

Journal of Alloys and Compounds

journal homepage: www.elsevier.com/locate/jallcom

Structural and optical properties of electrodeposited ZnO thin films on conductive RuO_2 oxides

Yuan-Chang Liang [a,*], M.Y. Tsai [b], Chiem-Lum Huang [a], Chia-Yen Hu [a], C.S. Hwang [b]

[a] Institute of Materials Engineering, National Taiwan Ocean University, Keelung 20224, Taiwan
[b] Department of Mechanical Engineering, Chienkuo Technology University, Changhua 500, Taiwan

ARTICLE INFO

Article history:
Received 30 September 2010
Received in revised form 5 December 2010
Accepted 8 December 2010
Available online 16 December 2010

Keywords:
Ceramics
Thin films
Crystal structure
Microstructure

ABSTRACT

ZnO thin films were grown on the 150 nm-thick RuO_2-coated SiO_2/Si substrates by electrochemical deposition in zinc nitrate aqueous solution with various electrolyte concentrations and deposition currents. Crystal orientation and surface structure of the electrodeposited ZnO thin films were characterized by X-ray diffraction (XRD) and scanning electron microscopy, respectively. The XRD results show the as-electrodeposited ZnO thin films on the RuO_2/SiO_2/Si substrates have mixed crystallographic orientations. The higher electrolyte concentration results in the ZnO thin films with a higher degree of *c*-axis orientation. Moreover, the use of an ultra-thin 5 nm-thick ZnO buffer layer on the RuO_2/SiO_2/Si substrate markedly improves the degree of preferential *c*-axis orientation of the electrodeposited ZnO crystalline. The subsequent annealing in vacuum at a low temperature of 300 °C reduces the possible hydrate species in the electrodeposited films. The electrodeposited ZnO thin films on the 5 nm-thick ZnO buffered RuO_2/SiO_2/Si substrates grown in 0.02 M electrolyte at −1.5 mA with a subsequent annealing in vacuum at 300 °C had the best structural and optical properties. The UV to visible emission intensity ratio of the film can reach 7.62.

1. Introduction

ZnO is a wide band gap semiconductor with a high exciton binding energy (60 meV) at room temperature. It is one of the technologically important oxide materials because of its versatile physical properties [1–4]. ZnO in thin film or nanostructured morphology is highly demanded for technological applications, especially for the use in various electronic and optoelectronic devices [5,6]. Many growth techniques have been adopted to prepare ZnO thin films and nanostructures, such as aqueous solution deposition [7,8], sol–gel process [9], molecular beam epitaxy [10], metal–organic vapor-phase epitaxy [6], and sputtering [2,4]. Among all methods, electrodeposition in aqueous solutions is a low cost method for preparation of large area thin films, in terms of its low-temperature process and arbitrary substrate shapes. It is well suited for mass production of semiconductor thin films. However, substrates for growing ZnO thin films or nanostructures by electrodeposition are most limited to metal substrates. Copper, platinum, gold, and zinc foil substrates have been demonstrated to be good substrate materials for electrodeposition of ZnO with various morphologies [11–15]. Most oxide materials are known to have a high electric resistance and are not suitable for the electrode materials to grow ZnO thin films or nanostructures by electrodeposition. The Sn-doped In_2O_3 thin film coated glass substrate is the commonly used working electrode for preparing electrodeposited ZnO thin films or nanostructures [16].

Among various oxide materials, RuO_2 is a good electrical contact material and it has a low electric resistivity of ~35 μΩ cm [17]. It processes a good thermal stability and has been used as diffusion barrier for growing various oxide materials [18–20]. Recently, the transparent RuO_2 contacts on ZnO thin films are fabricated for ZnO-based optoelectronic devices through sputtering and annealing processes [21]. However, the related studies on the use of such transparent conductive oxide for electrodepositing of ZnO are lacking. In this study, sputtering deposited conductive RuO_2 was used as working electrode to electrodeposited ZnO thin films. The correlation between the electrodeposition condition and structural properties of the ZnO thin films grown on RuO_2 is investigated. The effects of an ultra-thin ZnO buffer and a subsequent annealing procedure on the structure and optical properties of the electrodeposited ZnO thin films are discussed in this work.

2. Experimental

ZnO thin films were grown by cathodic electrochemical deposition from aqueous solutions containing $Zn(NO_3)_2$ at concentrations ranging from 0.004 M to 0.02 M. The bath temperature is maintained at 90 °C during the electrodeposition of ZnO. A standard three-electrode compartment cell was used in this experiment. A platinum

* Corresponding author.
E-mail addresses: yuanvictory@gmail.com, deanvera@yahoo.com.tw (Y.-C. Liang).

0925-8388/$ – see front matter © 2011 Elsevier B.V. All rights reserved.
doi:10.1016/j.jallcom.2010.12.059

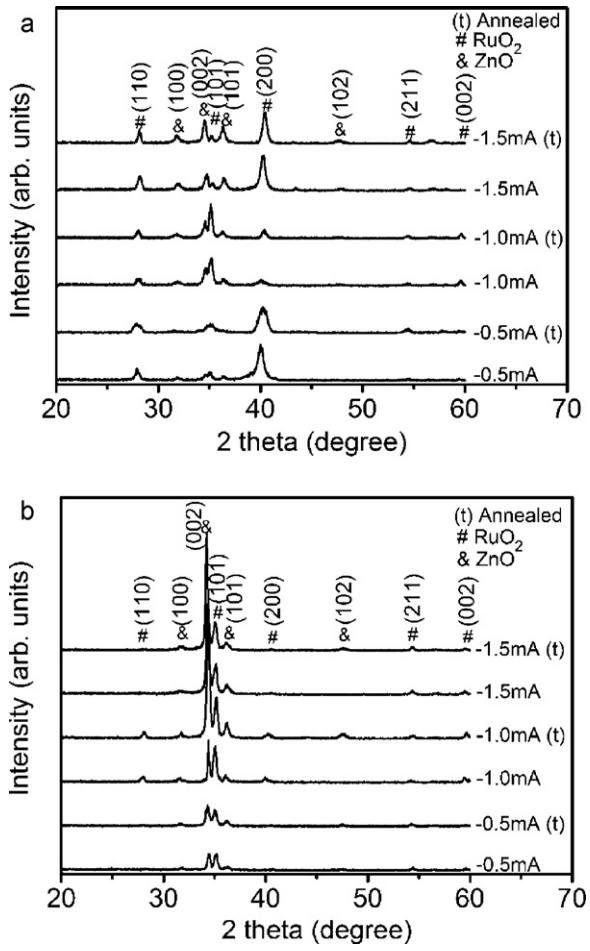

Fig. 1. XRD patterns of the electrodeposited ZnO thin films grown at various zinc nitrate concentrations and deposition currents on the $RuO_2/SiO_2/Si$ substrates. The symbol (t) represents the films are annealed in vacuum at 300 °C: (a) 0.004 M and (b) 0.02 M electrolytes.

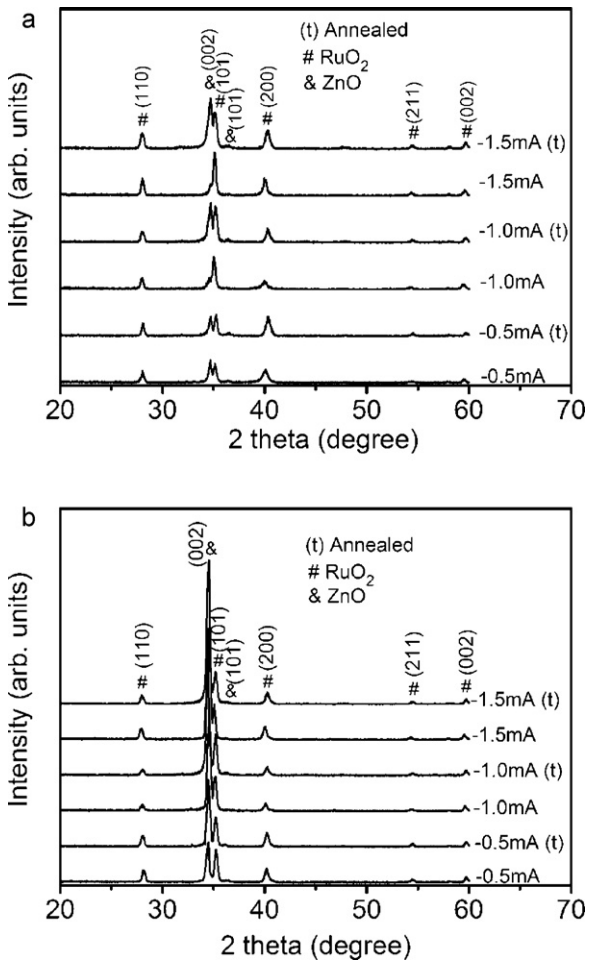

Fig. 2. XRD patterns of the electrodeposited ZnO thin films grown at various zinc nitrate concentrations on the $RuO_2/SiO_2/Si$ substrates with a 5 nm-thick ultra-thin ZnO buffer. The symbol (t) represents the films are annealed in vacuum at 300 °C: (a) 0.004 M and (b) 0.02 M electrolytes.

sheet (99.99%) and a 150 nm-thick RuO_2-coated/SiO_2/Si substrate (or 5 nm-thick ZnO buffered RuO_2 (150 nm)/SiO_2/Si) were used as the anode and cathode, respectively. A Ag/AgCl electrode in a saturated KCl solution was used as a reference electrode. The area of the substrate in the electrolyte for the electrodeposition is fixed at 1 cm^2. The deposition was performed at various deposition currents from −0.5 mA to −1.5 mA with respect to the reference electrode. Some of the as-electrodeposited ZnO thin films are subsequently annealed at 300 °C in vacuum for 30 min to evaluate the annealing effects on structure and optical properties of the films. The conductive 150 nm-thick RuO_2 thin films and ultra-thin ZnO buffer layers (5 nm thick) were prepared by radio-frequency magnetron sputtering. During depositions for the RuO_2 and ZnO buffer layers, the substrate temperatures were maintained at 450 °C and 250 °C, respectively. The pressure of working gas during deposition of RuO_2 thin films was fixed at 15 mTorr with an Ar/O_2 ratio of 8:2 and that for the ultra-thin ZnO layer is 15 mTorr with an Ar/O_2 ratio of 1:1.

The crystal structure of the electrodeposited ZnO thin films was characterized by X-ray diffraction (XRD). The surface morphology of the electrodeposited ZnO thin films was investigated by a scanning electron microscope (SEM). X-ray photoelectron spectroscope (XPS) measurements were performed to evaluate the energy state of the elements. The room temperature dependent photoluminescence (PL) spectra are obtained using the 325 nm line of a He–Cd laser.

Table 1
XRD peak intensity ratio $I_{(002)}/[I_{(100)}+I_{(002)}+I_{(101)}+I_{(102)}]$ of the ZnO thin films. The background intensity was deducted before the calculation of peak intensity ratio. The symbol (t) represents the films are annealed in vacuum at 300 °C.

Current (mA)	Conditions			
	0.004 M/RuO_2	0.004 M/RuO_2(t)	0.02 M/RuO_2	0.02 M/RuO_2(t)
−0.5	0.46	0.55	0.70	0.63
−1.0	0.59	0.60	0.77	0.81
−1.5	0.42	0.45	0.87	0.88
Current (mA)	Conditions			
	0.004 M/buffer	0.004 M/buffer(t)	0.02 M/buffer	0.02 M/buffer(t)
−0.5	0.92	0.86	0.96	0.97
−1.0	0.92	0.93	0.99	0.98
−1.5	0.89	0.93	0.99	0.99

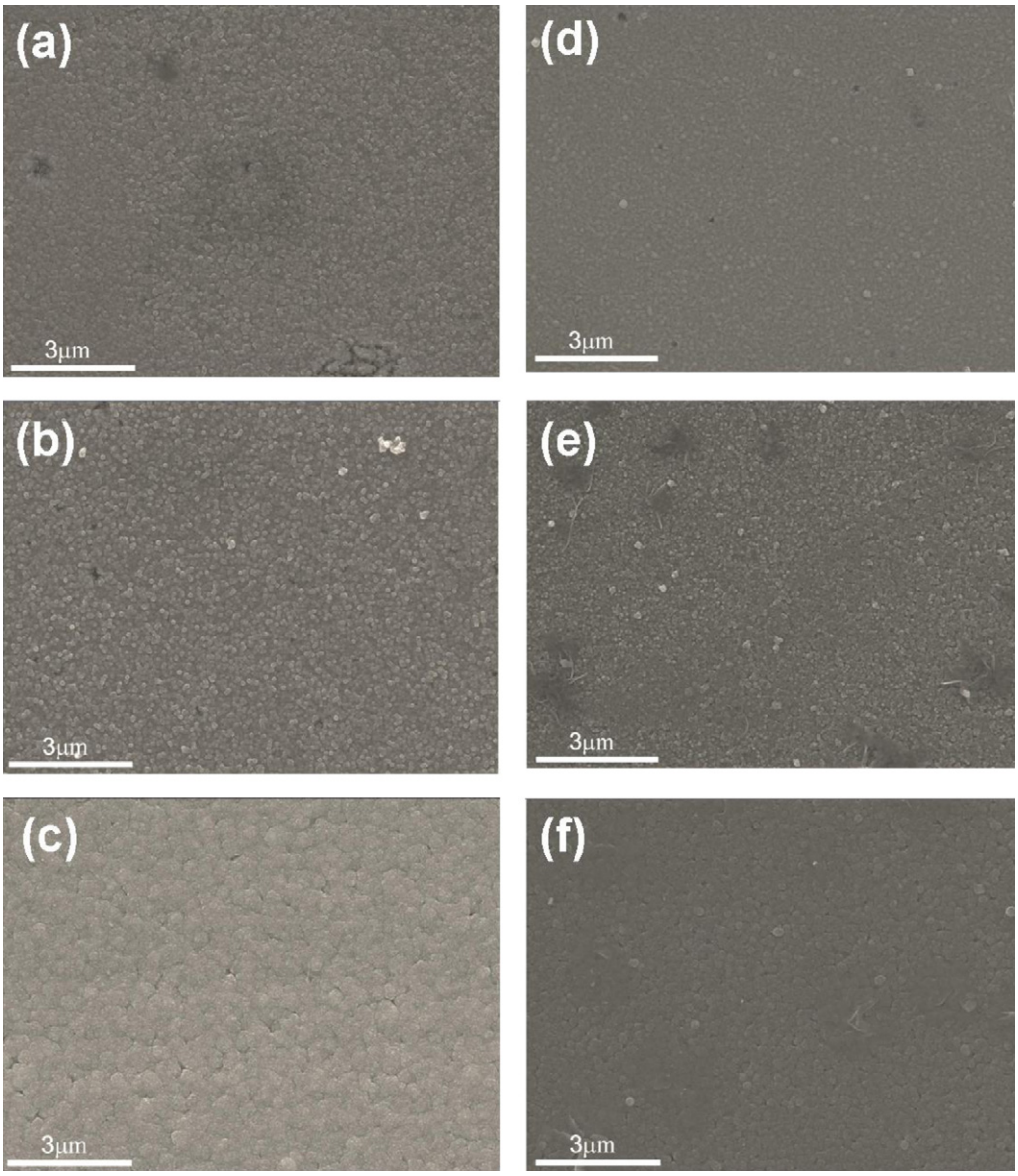

Fig. 3. SEM images of the annealed electrodeposited ZnO thin films grown at various zinc nitrate concentrations and deposition currents on the $RuO_2/SiO_2/Si$ substrates. (a) 0.004 M at −0.5 mA, (b) 0.004 M at −1.0 mA, (c) 0.004 M at −1.5 mA, (d) 0.02 M at −0.5 mA, (e) 0.02 M at −1.0 mA, and (f) 0.02 M at −1.5 mA.

3. Results and discussion

Fig. 1 shows the XRD patterns for the electrodeposited ZnO thin films on the $RuO_2/SiO_2/Si$ substrates. The ZnO thin films grown in the zinc nitrate solution with concentrations of 0.004 M and 0.02 M show a mixed crystallographic feature. The Bragg reflections of ZnO (1 0 0), (0 0 2), (1 0 1), and (1 0 2) are observed in the XRD patterns according to the examination from hexagonal ZnO JCPDS 36-1451. There are no clear Bragg's reflections from Zn or zinc hydroxide-related phases in the XRD patterns. The higher bath temperature is reported to further decreases the free energy of the reaction $Zn(OH)_2 \rightarrow ZnO + H_2O$ (−3.6 kJ/mol at 40 °C and −6.4 kJ/mol at 100 °C) [8]. The high bath temperature of 90 °C herein might help to decrease the degree of the possible formation of zinc hydroxide-related crystallites in the electrodeposited ZnO thin films. The peak intensity ratios of (0 0 2) Bragg's reflection to all crystallographic planes i.e., $I_{(002)}/[I_{(100)} + I_{(002)} + I_{(101)} + I_{(102)}]$ in the polycrystalline ZnO thin films are calculated and listed in Table 1. Background intensity of the Bragg reflections was deducted before the calculation of intensity ratio of Bragg's peaks. From Table 1, the peak intensity ratios are 0.42–0.59 for the ZnO films grown in 0.004 M electrolyte and those for the films grown in 0.02 M electrolyte are 0.7–0.87. The Bragg reflections of ZnO (0 0 2) are dominant among the crystallographic planes in the electrodeposited ZnO thin films herein. Moreover, the deposition current did not cause marked change in preferentially crystallographic orientation. The (0 0 2)-oriented electrodeposited ZnO thin films have been prepared at the bath temperature of 70 °C [22]. From the chemical reaction process, the reduction of NO_3^- results in the increase of OH^- ionic concentration in the aqueous solution. Accordingly, OH^- and Zn^{2+} will form $Zn(OH)_2$ on the cathode electrode. The $Zn(OH)_2$ will then be decomposed and form ZnO on the substrate. The amount of Zn ions in the electrolyte during deposition will be influenced by the electrolyte concentration. The lower concentration in the electrolyte leads to a lower deposition rate as dominated by the reaction $Zn^{2+} + 2OH^- \rightarrow Zn(OH)_2$. Hence, a relatively high concentration of zinc nitrate significantly enhanced the amount of (0 0 2)-oriented grain in the electrodeposited polycrystalline ZnO thin films. The subsequent annealing in vacuum increased the intensity of Bragg's reflections of the ZnO thin films, indicating

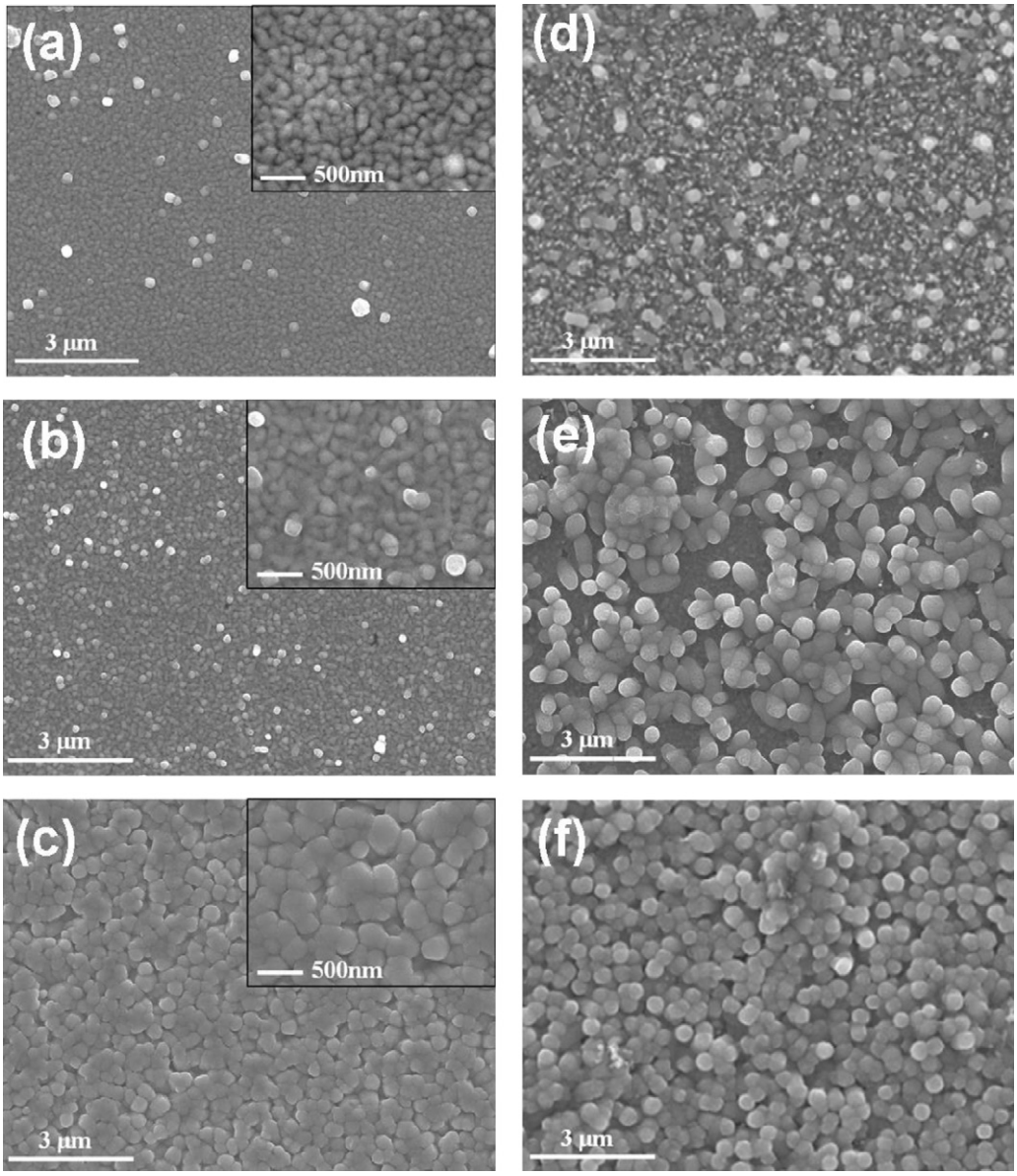

Fig. 4. SEM images of the annealed electrodeposited ZnO thin films grown at various zinc nitrate concentrations and deposition currents on the 5 nm-thick ZnO buffered $RuO_2/SiO_2/Si$ substrates. (a) 0.004 M at −0.5 mA, (b) 0.004 M at −1.0 mA, (c) 0.004 M at −1.5 mA, (d) 0.02 M at −0.5 mA, (e) 0.02 M at −1.0 mA, and (f) 0.02 M at −1.5 mA.

an increase in crystalline quality of the films. Furthermore, the peak intensity ratio of (0 0 2) Bragg's reflection to all crystallographic planes in the electrodeposited ZnO thin films is nearly the same after annealing process as exhibited in Table 1. This might be due to the annealing temperature is not high enough to cause the post growth of the ZnO grains to change the crystallographic texture properties. In contrast, the electrodeposited ZnO thin films grown on the 5 nm-thick ZnO buffered $RuO_2/SiO_2/Si$ substrates show a highly (0 0 2)-textured structure (Fig. 2). The ultra-thin ZnO buffer layer effectively reduces the crystallographic randomness of the electrodeposited ZnO thin films on the $RuO_2/SiO_2/Si$ substrates. The peak intensity ratios for the ZnO thin films grown in 0.004 M electrolyte are 0.89–0.92; there are quite a few portion of (1 0 1)-oriented grains in the ZnO thin films. Moreover, those for the films grown in 0.02 M electrolyte are 0.96–0.99. Nearly preferred *c*-axis orientation was observed in the ZnO crystalline films. The use of ultra-thin ZnO buffer layer on the $RuO_2/SiO_2/Si$ substrates effectively enhanced the growth characterization of the electrodeposited ZnO thin films along the *c*-axis direction. The subsequent annealing improved the intensity of the Bragg reflections of the ZnO thin films with less change in crystallographic texture properties.

The surface morphology of the electrodeposited ZnO thin films is not changed after the thermal annealing at 300 °C in vacuum. The SEM images of the post-annealed ZnO thin films are shown herein for a discussion. Fig. 3(a)–(c) displays the surface evolution of the electrodeposited ZnO thin films grown in the 0.004 M electrolyte under various deposition currents. The tiny grains packed closely for the ZnO thin films at −0.5 mA and −1.0 mA; the surface of the films is dense. Only few coarser ZnO grains are formed and distributed separately on the film surface. In contrast, coarse ZnO grains were formed for the film grown at −1.5 mA. The size of ZnO grains in the films increased with the deposition current. Fig. 3(d)–(f) shows the surface evolution of the ZnO thin films grown in the 0.02 M electrolyte under various deposition currents. The surface morphologies of the ZnO thin films are different from those grown in a relatively dilute electrolyte concentration. Under low deposition current of −0.5 mA, the surface morphology of the ZnO thin film has grains with two different morphologies. The surface

Table 2
Zn/O atomic ratio of the electrodeposited ZnO thin films derived from the narrow scans of XPS spectra. The symbol (t) represents the films are annealed in vacuum at 300 °C.

Zn/O/atomic ratio	Conditions			
	0.004 M/RuO_2	0.004 M/RuO_2(t)	0.02 M/RuO_2	0.02 M/RuO_2(t)
−0.5 mA (Zn/O)	0.89	0.90	0.94	0.95
−1.0 mA (Zn/O)	0.93	0.93	0.95	0.94
−1.5 mA (Zn/O)	0.96	0.94	0.98	0.98

of the ZnO thin film is composed of whisker-like tiny grains and the rod-like grains. These whisker-like ZnO grains might be the nuclei for the further growth of rod-like ZnO grains. Further increasing the deposition current to −1.0 mA, the ZnO thin film was covered with rod-like ZnO grains which size is larger than that of the film grown at −0.5 mA. However, these rod-like ZnO grains are not packed densely. The surface morphology of the ZnO thin film grown at −1.5 mA shows a dense and a uniform distribution of rod-like ZnO grains. The observation is consistent with the previous report that an increase in deposition current density causes the ZnO pillars to coalesce to form a dense nanopillar film [16]. Fig. 4 shows the SEM surface morphology of the ZnO thin films grown on the ultra-thin ZnO buffered $RuO_2/SiO_2/Si$ substrates. Comparatively, the ZnO thin films grown on the ultra-thin ZnO buffered $RuO_2/SiO_2/Si$ substrates show a dense and homogeneous surface morphology with respect to those on the $RuO_2/SiO_2/Si$ substrates. The surface of the ZnO thin films grown on the ultra-thin ZnO buffered $RuO_2/SiO_2/Si$ substrates is smoother than that grown on the $RuO_2/SiO_2/Si$ substrate at a given electrodeposition condition. Liu et al. reported that the coverage density and morphology of the electrodeposited ZnO thin films are related to the lattice structure and defects on the substrate surface, which are key factors for subsequent thin film nucleation and growth during electrodeposition [23]. The thin native ZnO layer on the Zn metal substrate was reported to enhance nucleation and allow more highly aligned, dense ZnO structures to be grown [14]. The ultra-thin ZnO buffer layer on the $RuO_2/SiO_2/Si$ improves the homogeneous nucleation of the electrodeposited ZnO thin films and further increases the flatness of the electrodeposited ZnO film surface.

XPS was used to determine the composition of the ZnO thin films and the effects of annealing on chemical state of the constituent elements. The calculated atomic concentrations of Zn and O are listed in Table 2. The samples for the XPS measurements herein were pre-sputtered with Ar^+ ions for duration of 1 min. The atomic ratio of Zn/O increases slightly with the deposition current density and the concentration of electrolyte. The atomic ratios of Zn/O for the electrodeposited ZnO thin films herein are below 1.0, revealing the compositions of the ZnO thin films are non-stoichiometric with a zinc deficiency. The buffering of an ultra-thin ZnO on the $RuO_2/SiO_2/Si$ substrate did not cause a change of composition of the electrodeposited ZnO thin films. Fig. 5(a)–(c) shows the chemical bonding states of the Zn element in the electrodeposited ZnO thin films. All the samples have a symmetric $Zn2p_{3/2}$ XPS spectrum, revealing no excess Zn in the films [24]. Fig. 5(d)–(f) shows the ZnO thin films have a clear asymmetric curve of O1s spectrum. The lower binding energy component is attributed to oxygen in the oxide crystal [25] and the higher binding energy component represents oxygen ions in oxygen-deficient regions within the matrix of ZnO and/or the presence of hydrated oxide species corresponding to OH [26,27]. The ZnO thin film grown in the 0.004 M electrolyte at −0.5 mA has a largest area ratio (53.7%) of the higher binding energy component to the lower binding energy component. That area ratio for the ZnO thin film decreased with the concentration of zinc nitrate electrolyte (from 53.7% to 34.4% as the concentration of electrolyte was increased from 0.004 M to 0.02 M), revealing the crystalline quality of the ZnO thin film grown at a low current density was improved by increasing the concentration of electrolyte. The electrodeposited ZnO thin film that was further annealed in vacuum clearly shows a decrease in the area ratio of the higher binding component to the lower one. This can be attributed to the reduction of possible defects such as the hydrate species in the electrodeposited film [28].

The PL measurements are used to investigate the buffering and annealing effects on the optical properties of the electrodeposited ZnO thin films. The electrodeposited ZnO thin films grown in 0.02 M electrolyte are investigated herein because they are more stoichiometric in composition and highly *c*-axis oriented with respect to those of the films electrodeposited in 0.004 M electrolyte. Fig. 6(a)–(c) shows the PL spectra of the as-electrodeposited ZnO thin films on the $RuO_2/SiO_2/Si$ substrates with various deposition currents. The samples show a large and broad visible light luminescence centered at ~550–570 nm. This visible emission peak might be resulted from the defects of the films such as OH groups [29] or the oxygen vacancies [30]. The XPS results exhibit that the elec-

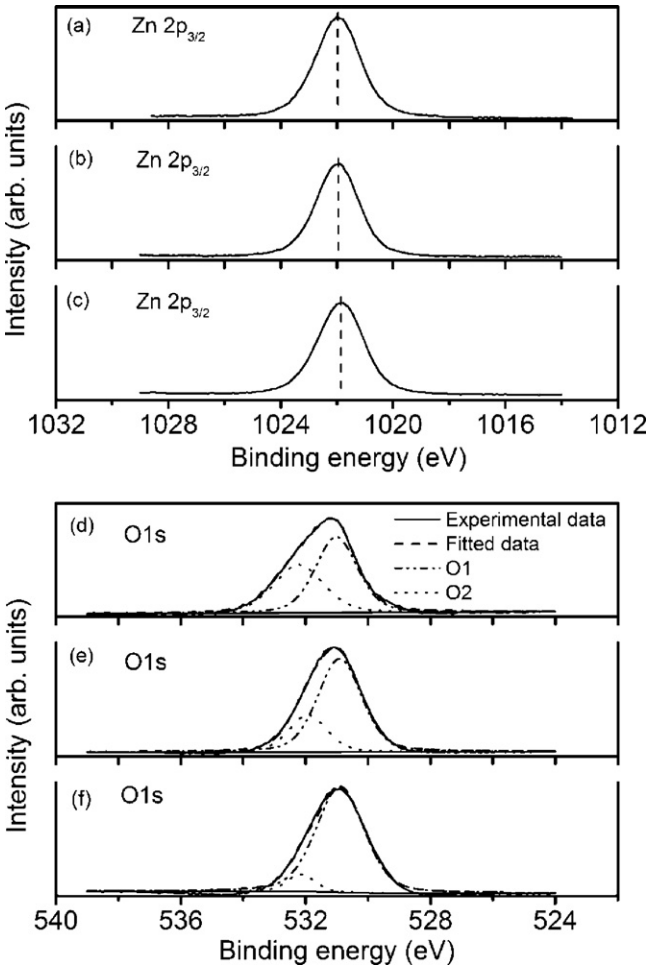

Fig. 5. XPS spectra of the $Zn2p_{3/2}$ ((a)–(c)) and O1s ((d)–(f)) for the electrodeposited ZnO thin films. (a) and (d): 0.004 M at −0.5 mA. (b) and (e): 0.02 M at −0.5 mA. (c) and (f): 0.02 M at −0.5 mA with a thermal annealing in vacuum at 300 °C.

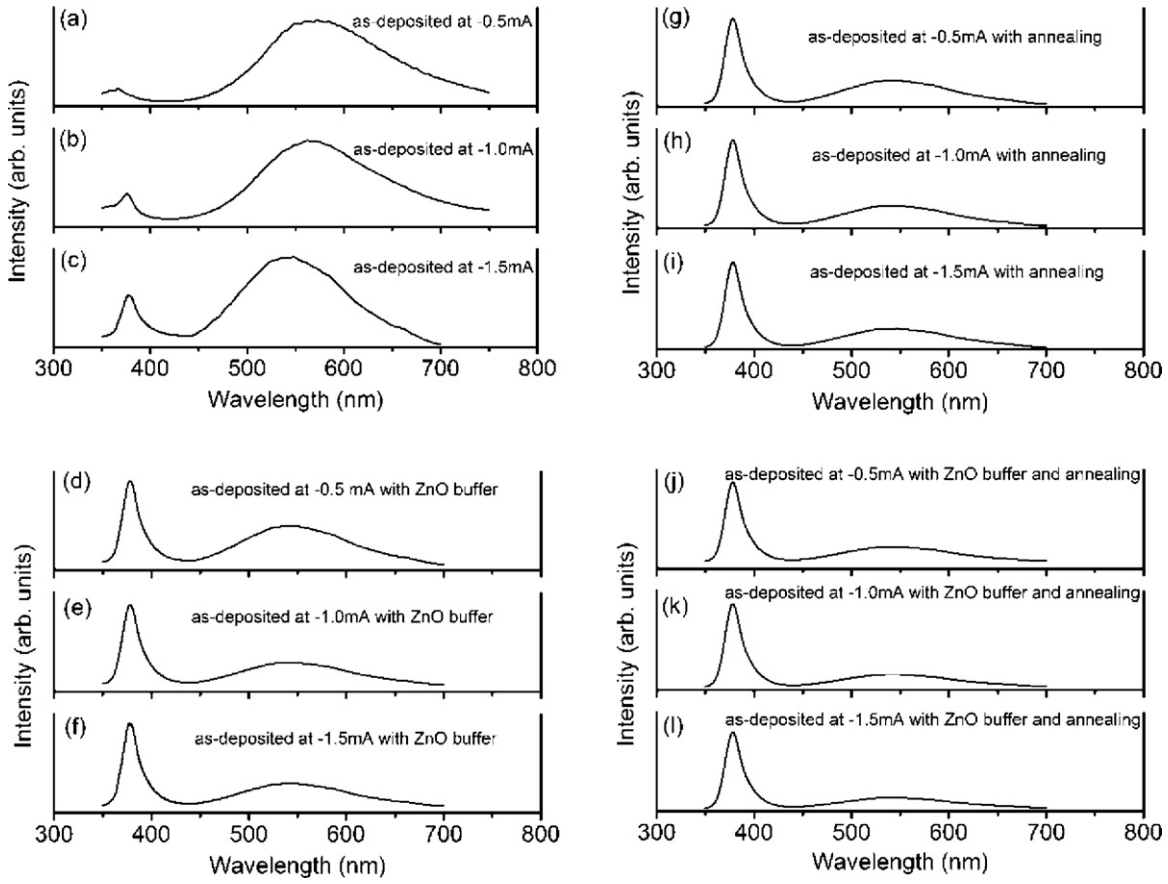

Fig. 6. PL spectra of the electrodeposited ZnO thin films grown in 0.02 M electrolyte at various deposition currents. (a) −0.5 mA, (b) −1.0 mA, and (c) −1.5 mA. The effects of the ultra-thin ZnO buffer on the PL spectra of the electrodeposited ZnO thin films without a thermal annealing are shown in (d)–(f). The effects of thermal annealing in vacuum on the PL spectra of the electrodeposited ZnO thin films on the $RuO_2/SiO_2/Si$ substrates are shown in (g)–(i). The PL spectra of the ZnO thin films grown at various deposition currents on the 5 nm-thick ZnO buffered $RuO_2/SiO_2/Si$ substrates with a thermal annealing in vacuum are shown in (j)–(l).

trodeposited ZnO thin films might have the oxygen vacancies and hydrated oxide species in the films even though the film is annealed in vacuum. The PL peak corresponding to UV emission of the ZnO thin films was observed to increase with increasing the deposition current. This can be attributed to the increase of deposition current results in the enhancement of ZnO *c*-axis texture as exhibited in the XRD patterns. A clear PL peak of UV emission was posited to the high quality of the (0 0 2)-textured nanostructured ZnO film [31,32]. A clear UV emission of PL spectra was observed for the electrodeposited ZnO thin films on the 5 nm-thick ZnO buffered $RuO_2/SiO_2/Si$ substrates (Fig. 6(d)–(f)). The UV to visible ratio of the PL spectra herein was defined as the ratio of the maximum intensities of the UV and visible peaks and was used to compare the crystal quality of the ZnO thin films. The UV to visible ratio of all samples is shown in Fig. 7. The values of UV to visible ratio for the as-electrodeposited ZnO thin films without an ultra-thin ZnO buffer are below 1.0. Comparatively, the ratio was largely increased to 2.16–3.9 when an ultra-thin ZnO buffer was used. The ultra-thin ZnO buffer layer enhances not only the (0 0 2)-preferred orientation but also the surface flatness of the electrodeposited ZnO thin films. The use of ultra-thin ZnO buffer for the growth of electrodeposited ZnO thin films on the $RuO_2/SiO_2/Si$ substrates helps to reduce possible defects which might be easily generated when the rod-like ZnO thin films were formed without a ZnO buffer layer on the $RuO_2/SiO_2/Si$ substrates. The optical properties of the ZnO thin films have been investigated with different degrees of crystal quality [33]. The enhancement of UV emission of ZnO thin films with a thin homointerlayer has been demonstrated in sputtering deposited ZnO thin films on $SrTiO_3$ substrates and pulsed laser deposited ZnO thin films on sapphire substrates [2,34]. Moreover, the relative peak intensity of visible emission of the electrodeposited ZnO thin films without a ZnO buffer layer is also markedly decreased with a thermal annealing in vacuum. Fig. 6(g)–(i) shows the PL spectra of the electrodeposited ZnO thin films annealed in vacuum at 300 °C without ZnO buffering. The values of UV to visible ratio for ZnO thin films annealed in vacuum at 300 °C are 3.34, 3.88, and 4.21 for

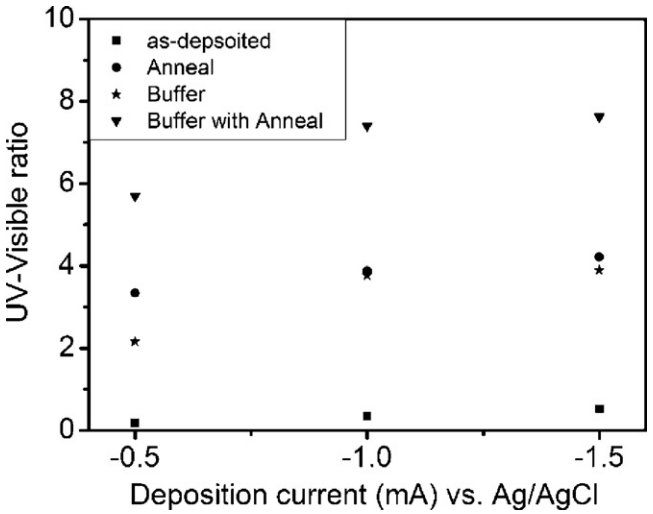

Fig. 7. UV-to-visible emission intensity ratio of the electrodeposited ZnO thin films. The data were derived from the PL spectra of Fig. 6.

the films grown at −0.5 mA, −1.0 mA, and −1.5 mA, respectively. The increased UV to visible ratio of the annealed electrodeposited ZnO thin films might be associated with the elimination of most possible hydroxyl groups in the electrodeposited films [35]. This can be confirmed with the XPS results that the area of the defect-related component in O1s spectrum was reduced after annealing. The improvement of UV emission of the ZnO thin films by annealing was also reported in literatures [36]. However, some defects were still present after annealing incurring a visible emission. Fig. 6(j)–(l) shows the PL spectra of the electrodeposited ZnO on the ultra-thin ZnO buffered $RuO_2/SiO_2/Si$ substrates annealed in vacuum at 300 °C. The UV to visible ratio was largely enhanced from 0.19 to 5.69 for the as-deposited ZnO thin film grown at −0.5 mA and that with a buffer layer annealed in vacuum, respectively. The electrodeposited ZnO thin films grown on the ZnO buffered $RuO_2/SiO_2/Si$ substrates at −1.0 mA and −1.5 mA and with thermal annealing have high values of UV to visible ratio of 7.4–7.62. The experimental results herein concluded that an ultra-thin ZnO buffer layer can effectively improve the *c*-axis texture of the electrodeposited ZnO thin films and the film morphology can be transformed from the rod-like to the dense and flat film surface. The electrodeposition is conducted at a relatively low temperature compared to that of other vacuum deposition methods and in an electrolyte that induces a large amount of hydrate species in electrodeposited ZnO thin films. The subsequent thermal annealing in vacuum at a low temperature of 300 °C further reduced the contamination of hydrate species in the electrodeposited films. The adoption of an ultra-thin ZnO homointerlayer and a subsequent annealing realized the fabrication of the ZnO thin films on the $RuO_2/SiO_2/Si$ substrates with good optical properties by electrodeposition in aqueous solution.

4. Conclusions

ZnO thin films on the $RuO_2/SiO_2/Si$ substrates were prepared by electrodeposition in aqueous zinc nitrate solutions. The $ZnO/RuO_2/SiO_2/Si$ thin films grown in 0.004 M and 0.02 M electrolytes under various deposition currents show a mixed crystallographic feature. The XRD results show the ultra-thin ZnO buffer layer effectively reduces the crystallographic randomness of the electrodeposited ZnO thin films on the $RuO_2/SiO_2/Si$ substrates. An ultra-thin ZnO buffer layer on the $RuO_2/SiO_2/Si$ improves the homogeneous nucleation of the electrodeposited ZnO thin films and further enhances the flatness of ZnO film surface. The subsequent annealing of the electrodeposited ZnO thin films in vacuum substantially reduced the amount of hydroxyl defects in the electrodeposited films. The PL spectra reveal that both the ultra-thin ZnO buffer layer and a subsequent thermal annealing can improve the crystal quality of the electrodeposited ZnO thin films on the $RuO_2/SiO_2/Si$ substrates. The ZnO thin films grown on the $RuO_2/SiO_2/Si$ substrates with good optical properties can be realized with the thin-homolayer buffering and an adequate thermal annealing.

Acknowledgements

This work is supported by the National Taiwan Ocean University (Grant No. NTOU-RD-AA-2010-104031) and the National Science Council of the Republic of China (Grant No. NSC 99-2221-E-019-055).

References

[1] S. Liang, H. Sheng, Y. Liu, Z. Hio, Y. Lu, H. Shen, J. Cryst. Growth 225 (2001) 110.
[2] Y.C. Liang, J. Alloys Compd. 508 (2010) 158.
[3] J.Y. Lee, Y.S. Choi, J.H. Kim, M.O. Park, S. Im, Thin Solid Films 403 (2002) 533.
[4] Y.C. Liang, C.C. Liu, C.C. Kuo, Y.C. Liang, J. Cryst. Growth 310 (2008) 3741.
[5] J.S. Lee, M.S. Islam, S. Kim, Nano Lett. 6 (2006) 1487.
[6] W.I. Park, G.C. Yi, Adv. Mater. 16 (2004) 87.
[7] M. Izaki, T. Omi, J. Electrochem. Soc. 144 (1997) L3.
[8] S. Peulom, D. Lincot, J. Electrochem. Soc. 145 (1998) 864.
[9] L. Vayssieres, K. Keis, S.-E. Lindquist, A. Hagfeldt, J. Phys. Chem. B 105 (2001) 3350.
[10] M. Sano, K. Miyamoto, H. Kato, T. Yao, J. Appl. Phys. 95 (2004) 5527.
[11] G.R. Li, C.R. Dawa, Q. Bu, F.L. Zhen, X.H. Lu, Zh.H. Ke, H.E. Hong, Ch.Zh. Yao, P. Liu, Y.X. Tong, Electrochem. Commun. 9 (2007) 863.
[12] G. Machado, D.N. Guerra, D. Leinen, J.R. Ramos-Barrado, R.E. Marotti, E.A. Dalchiele, Thin Solid Films 490 (2005) 124.
[13] S.J. Lee, S.K. Park, C.R. Park, J.Y. Lee, J. Park, Y.R. Do, J. Phys. Chem. C 111 (2007) 11793.
[14] M.H. Wong, A. Berenov, X. Qi, M.J. Kappers, Z.H. Barber, B. Illy, Z. Lockman, M.P. Ryan, J.L. MacManus-Driscoll, Nanotechnology 14 (2003) 968.
[15] A. Ashida, A. Fujita, Y. Shim, K. Wakita, A. Nakahira, Thin Solid Films 517 (2008) 1461.
[16] Q.P. Chen, M.Z. Xue, Q.R. Sheng, Y.G. Liu, Z.F. Ma, Electrochem. Solid-State Lett. 9 (2006) C58.
[17] W.D. Ryden, A.W. Lawson, C.C. Sartain, Phys. Rev. B 1 (1970) 1494.
[18] R.G. Vadimsky, R.P. Frankenthal, D.E. Thompson, J. Electrochem. Soc. 126 (1979) 2017.
[19] Y.C. Liang, Y.C. Liang, Thin Solid Films 518 (2010) S17.
[20] Y.C. Liang, J. Cryst. Growth 312 (2010) 1610.
[21] T.K. Lin, S.J. Chang, B.R. Huang, K.T. Lam, Y.S. Sun, M. Fujita, Y. Horikoshi, J. Electrochem. Soc. 153 (2006) G677.
[22] S. Otani, J. Katayama, H. Umemoto, M. Matsuoka, J. Electrochem. Soc. 153 (2006) C551.
[23] X. Liu, Z. Jin, S. Bu, J. Zhao, Z. Liu, Mater. Lett. 59 (2005) 3994.
[24] M.N. Islam, T.B. Ghosh, Thin Solid Films 280 (1996) 20.
[25] R. Cebulla, R. Werndt, K. Ellmer, J. Appl. Phys. 83 (1998) 1087.
[26] J.C.C. Fan, J.B. Goodenough, J. Appl. Phys. 48 (1977) 3524.
[27] S.B. Majumder, M. Jain, P.S. Dobal, R.S. Katiyar, Mater. Sci. Eng. B 103 (2003) 16.
[28] L. Zhang, Z. Chen, Y. Tang, Z. Jia, Thin Solid Films 492 (2005) 24.
[29] N.S. Norberg, D.R. Gamelin, J. Phys. Chem. B 109 (2005) 20810.
[30] Y. Li, G.W. Meng, L.D. Zhang, F. Phillip, Appl. Phys. Lett. 76 (2002) 2011.
[31] B. Cao, Y. Li, G. Duan, W. Cai, Cryst. Growth Des. 6 (2006) 1091.
[32] K.H. Tam, C.K. Cheung, Y.H. Leung, A.B. Djurisic, C.C. Ling, C.D. Beling, S. Fung, W.M. Kwok, W.K. Chan, D.L. Phillips, L. Ding, W.K. Ge, J. Phys. Chem. B 110 (2006) 20865.
[33] Y.R. Ryu, S. Zhu, J.M. Wrobel, H.M. Jeong, P.F. Miceli, H.W. White, J. Cryst. Growth 216 (2000) 326.
[34] H.S. Kim, S.J. Pearton, D.P. Norton, F. Ren, Appl. Phys. A 91 (2008) 255.
[35] R. Xie, T. Sekiguchi, T. Ishigaki, N. Ohashi, D. Li, D. Yang, B. Liu, Y. Bando, Appl. Phys. Lett. 88 (2006) 134103.
[36] B. Marí, F.J. Manjón, M. Mollar, J. Cembrero, R. Gómez, Appl. Surf. Sci. 252 (2006) 2826.